Z. Phys. Chem. **227** (2013) 1421–1433 / **DOI** 10.1524/zpch.2013.0401

Exploring Pathways of Photoaddition Reactions by Artificial Force Induced Reaction Method: A Case Study on the Paternò–Büchi Reaction

By Satoshi Maeda[1,*], Tetsuya Taketsugu[1], and Keiji Morokuma[2,3,*]

[1] Department of Chemistry, Faculty of Science, Hokkaido University, Sapporo 060-0810, Japan
[2] Fukui Institute for Fundamental Chemistry, Kyoto University, Kyoto 606-8103, Japan
[3] Department of Chemistry and Cherry L. Emerson Center for Scientific Computation, Emory University, Atlanta, GA 30322, USA

(Received February 8, 2013; accepted in revised form April 27, 2013)
(Published online June 17, 2013)

Automatic Search / Reaction Pathway / Artificial Force Induced Reaction Method / AFIR Method / Photoaddition Reaction / Paternò–Büchi Reaction

The present study demonstrates *a priori* prediction of the mechanism of Paternò–Büchi (PB) reaction by automated search for reaction pathways using the artificial force induced reaction (AFIR) method, for the simplest set of reactants, $H_2CO + C_2H_4$. The search found all previously suggested pathways automatically without using any guess about the reaction mechanism. Even the reaction product was not assumed. In addition, a comprehensive view of the reaction path network obtained in the present extensive search gave new insights into the mechanism. Barriers on excited states explained the preference of the initial bonding sites. A seam of crossing between the lowest triplet and first singlet excited state is suggested to make a significant contribution to an intersystem crossing and the reaction mechanism of the present system.

1. Introduction

Finding structures of the transition states (TSs) is a key for understanding the mechanism of chemical reactions. The geometry of TS can be obtained as the first-order saddle point on the potential energy surface (PES) [1]. Hence, considerable efforts have been made in development of efficient methods for finding first-order saddles on given PESs. These include geometry optimization techniques, double-ended methods, coordinate driving approaches, *etc.*, and are reviewed in Refs. [2–4]. Once a TS is obtained, the intrinsic reaction coordinate (IRC) can be computed as the mass-weighted steepest descent path along the direction of imaginary frequency vibrational mode [5–10], and it has been considered as a chemical reaction path connecting reactant's local minimum with product well *via* the TS. Numerous chemical reactions have been studied theoretically with calculations of TSs and IRCs [11–15].

* Corresponding authors. E-mail: smaeda@mail.sci.hokudai.ac.jp; morokuma@fukui.kyoto-u.ac.jp

Another important concept in chemical reactions is the seam of crossing [16–19] (SX) between two or more PESs including the conical intersection [20–24] (CI) which is a special SX between states with the same spin and space symmetry. The degeneracy on SX is lifted by geometrical displacements toward the difference gradient vector (DGV) direction, while on CI a move along the derivative coupling vector (DCV) also lifts the degeneracy. Since the nonadiabatic transition takes place efficiently near SX and CI, identifying their locations is another significant task in studying chemical reactions theoretically. Thus, various techniques have been developed in order to locate minimum energy SX (MSX) and CI (MECI) geometries efficiently [17,25–32]. Nonadiabatic transitions can also occur in high energy regions of SX/CI depending on the topography of PES and excess energy, and hence, higher energy regions including first-order saddles and minimum energy paths within SX/CI hypersurface have also been calculated [30,32–35].

In general, it is still very difficult to predict reaction mechanisms *a priori*. This is because most of TS optimization methods and SX/CI search methods require some estimates about reaction mechanisms, such as guesses of TS and SX/CI structures, reaction variables, and products and key intermediates [2–4]. Thus, practical methods that can find all reaction pathways without any guess need to be developed. To achieve this goal, we have developed automated reaction path search methods under the title of global reaction route mapping (GRRM) strategy [36]. One of them, the artificial force induced reaction (AFIR) method [37,38], can efficiently explore pathways for $A + B \rightarrow X\,(+\,Y)$ type addition reactions, and thus is effective for study of complex organic and organometallic reactions [39–41]. Very recently, *a priori* prediction of the full catalytic cycle of an organometallic catalysis was achieved by AFIR. In the search, for reactions of three reactants, C_2H_4, CO, and H_2, and a catalyst $HCo(CO)_3$, the major product $CH_3CH_2C(O)H$ and all relevant TSs and intermediates were located efficiently (in less than 6 d on 2 CPUs) without any guess about its reaction mechanism [40].

It is interesting to explore the applicability of the AFIR method to *a priori* predictions of reaction mechanisms of electronically excited molecules. In this study, a photoaddition reaction between an aldehyde (or ketone) and an alkene known as Paternò–Büchi (PB) reaction [42–45] is considered. Its mechanism has been studied extensively both experimentally and theoretically [46–54]. Thus, this reaction is ideal for the present purpose of benchmarking the applicability to photochemical addition reactions. In contrast to the case of organometallic catalysis, not only ground state TSs but also excited state TSs, SXs, and CIs need to be found systematically. The present search located all relevant TSs, MSXs, and MECIs automatically and found the most favorable mechanism of the PB reaction *a priori*. Pathways obtained in the present study reproduced all the previously suggested mechanisms, and furthermore, indicated new insights into reaction mechanisms.

2. Method

2.1 Artificial force induced reaction method

The AFIR method applies artificial force between given reactants [37,38]. Thus, products of addition reactions between reactants A and B can be found very efficiently just

by minimizing the following model function called AFIR function,

$$F(\mathbf{Q}) = V(\mathbf{Q}) + \alpha \frac{\sum_{i\in A}\sum_{j\in B}\left[(R_i + R_j)/r_{ij}\right]^p r_{ij}}{\sum_{i\in A}\sum_{j\in B}\left[(R_i + R_j)/r_{ij}\right]^p} \tag{1}$$

where $V(\mathbf{Q})$ is the PES that depends on the atomic coordinates $\mathbf{Q} = \{Q_k\}$, r_{ij} is a distance between the ith and jth atoms in the reactants A and B, respectively, and summations are taken over all or selected pairs of atoms in A and B. The constant p is a parameter of inverse distance weighting [55] (set to a standard value [37] $p = 6$), and each inverse distance $1/r_{ij}$ is scaled by the sum of covalent radii $(R_i + R_j)$ of the ith and jth atoms, respectively, to take the difference in atomic size into account. The parameter α represents the strength of force, and for convenience it can be rewritten as,

$$\alpha = \frac{\gamma}{\left[2^{-\frac{1}{6}} - \left(1 + \sqrt{1 + \frac{\gamma}{\sigma}}\right)^{-\frac{1}{6}}\right] R_0} \tag{2}$$

where α is given as an average force acting on two atoms in the energy range $0 < E < \gamma$ when E is formally represented by the Lennard–Jones potential, and in practice we adopted R_0 and σ to be the values for argon clusters ($R_0 = 3.8164$ Å and $\sigma = 1.0061$ kJ/mol). The parameter γ is called model collision energy between two reactant particles, and provides the upper limit of the barrier height to be seen in the search.

Starting from a random or inputted orientation and direction between two molecules A and B, an approximate reaction product can be obtained by minimizing the AFIR function with a sufficiently large γ to overcome the reaction barrier. Since the minimization path called AFIR path typically goes through near the TS region, an approximate TS geometry is also obtained. These approximate geometries can easily be optimized to corresponding true minima and TSs by a standard geometry optimization technique. By repeating AFIR minimizations starting from many random or systematically generated structures, all pathways for addition reactions between A and B can be located automatically. Further details can be found in our previous papers [36–38].

2.2 Seam model function approach

In order to search for MSXs and MECIs by AFIR, a two-step procedure called seam model function (SMF) approach is employed [56–58]. Although SMF was originally introduced for another automated search method called anharmonic downward distortion following method [56], it can be combined with any method such as AFIR [57]. In the first step, AFIR is applied to the following model function $X(\mathbf{Q})$ (in place of PES $V(\mathbf{Q})$ in Eq. (1)), which consists of a mean energy term for target PESs $E^{\text{State1}}(\mathbf{Q})$ and $E^{\text{State2}}(\mathbf{Q})$ and a penalty function for their energy gap.

$$X(\mathbf{Q}) = \frac{1}{2}\left[E^{\text{State1}}(\mathbf{Q}) + E^{\text{State2}}(\mathbf{Q})\right] + \frac{\left[E^{\text{State1}}(\mathbf{Q}) - E^{\text{State2}}(\mathbf{Q})\right]^2}{\beta^{\text{SMF}}} \tag{3}$$

In Eq. (3), $\mathbf{Q}$ is the atomic coordinates $\{Q_k\}$ and β^{SMF} is a constant parameter which is set to a standard value ($\beta^{\mathrm{SMF}} = 30\,\mathrm{kJ/mol}$). Minimization of $X(\mathbf{Q})$ gives a geometry in which both the mean energy and the energy gap are small. Hence, minima on $X(\mathbf{Q})$ can be good guesses of MSXs and MECIs. It should be noted that similar penalty functions have been employed in MSX/MECI optimizations previously [28,29,31]. Since $X(\mathbf{Q})$ is a smooth single-valued function, AFIR or other automated reaction path search methods can readily be applied without modification. In other words, $V(\mathbf{Q})$ in Eq. (1) is simply replaced by $X(\mathbf{Q})$ in the first step of SMF/AFIR search. Then, in the second step, these approximate MSXs and MECIs on $X(\mathbf{Q})$ obtained by AFIR are optimized to true ones, using any optimization method; in the present case the direct gradient method [26,30,32] has been used. These two-step SMF/AFIR search gives many MSXs and MECIs automatically for photoaddition reactions.

2.3 Avoiding model function approach

Automated reaction path search methods for single PES such as AFIR cannot be applied directly to excited-state PES because of the existence of CIs in low energy regions. Therefore, another two-step strategy using the avoiding model function (AMF) approach is adopted [58]. In the first step, AFIR is applied to the following model function $Y(\mathbf{Q})$ that consists of a mean energy term for the target (higher) PES $E^{\mathrm{State1}}(\mathbf{Q})$ and the lower PES $E^{\mathrm{State2}}(\mathbf{Q})$ and a smoothing function.

$$Y(\mathbf{Q}) = \frac{1}{2}\left[E^{\mathrm{State1}}(\mathbf{Q}) + E^{\mathrm{State2}}(\mathbf{Q})\right] + \sqrt{\left[E^{\mathrm{State1}}(\mathbf{Q}) - E^{\mathrm{State2}}(\mathbf{Q})\right]^2 + 4\left[U(\mathbf{Q})\right]^2} \tag{4}$$

The function $U(\mathbf{Q})$ in the smoothing function is given as,

$$U(\mathbf{Q}) = \frac{\beta^{\mathrm{AMF}}}{2}\exp\left[-\left(\frac{E^{\mathrm{State1}}(\mathbf{Q}) - E^{\mathrm{State2}}(\mathbf{Q})}{\beta^{\mathrm{AMF}}}\right)^2\right] \tag{5}$$

where β^{AMF} is a constant parameter that is set to a standard value ($\beta^{\mathrm{AMF}} = 30\,\mathrm{kJ/mol}$). $U(\mathbf{Q})$ shifts the $Y(\mathbf{Q})$ value upward near CI regions, and smoothens singular regions of the upper PES associated with CIs. Therefore, AFIR can be applied directly to this smooth single-valued function. Moreover, $U(\mathbf{Q})$ rapidly decreases to zero away from CI regions, and thus $Y(\mathbf{Q})$ is very similar to $E^{\mathrm{State1}}(\mathbf{Q})$ except for CI regions. In other words, first-order saddle points obtained on $Y(\mathbf{Q})$ are very similar to those on $E^{\mathrm{State1}}(\mathbf{Q})$. Thus, approximate TSs obtained by AFIR on $Y(\mathbf{Q})$ are re-optimized to true TSs in the second step. This two-step AMF/AFIR search gives many TSs automatically for photoaddition reactions.

2.4 Computation

In this study, for the simplest $H_2CO + C_2H_4$ system, the singlet ground S_0, singlet first excited S_1, and lowest triplet T_1 states were considered. The initial SMF/AFIR and AMF/AFIR searches were made at the CASPT2/6-31G level with a six electrons and five orbitals [6e, 5o] active space. This active space can describe the n-π^* and π-π^*

excitations in H_2CO as well as the π-π^* excitation of C_2H_4 when the two species are separated. T_1 was calculated by single-state-(SS-)CASPT2. For singlet states, SS-CASPT2 was employed in the initial search for S_0 and S_0/T_1-SX structures, and the remaining S_1, S_0/S_1-CI, and S_1/T_1-SX structures were explored with multi-state-(MS-)CASPT2. The shift parameter 0.3 was employed to avoid the intruder state problem of CASPT2. Repetition of AFIR minimizations starting from random orientations and directions between H_2CO and C_2H_4 were terminated if the last 30 AFIR minimizations found no new product. The model collision energy parameter γ was set to 100 kJ/mol; pathways with barriers higher than ~100 kJ/mol are excluded in this search. Once two molecules are attached to each other on the excited states T_1 or S_1, pathways for the next step were searched on the S_0 state starting from S_0/T_1-MSX and S_0/S_1-MECI geometries, by minimizing the AFIR function from which terms $[(R_i + R_j)/r_{ij}]^p r_{ij}$ in Eq. (1) with high weight (with large $[(R_i + R_j)/r_{ij}]^p$) at the starting point is deleted. In Eq. (1), weight for terms associated with new O–C and C–C bonds almost exclusively dominate the AFIR function at S_0/T_1-MSX and S_0/S_1-MECI geometries. Thus, by eliminating these dominant terms at the initial structure and minimizing the AFIR function without such terms, further reaction steps can be explored. This treatment is similar to that taken in the previous application to the organometallic catalysis, where a substrate was reacted with ligands on the metal center by minimizing the AFIR function from which the term with dominant weight, *i.e.*, the term for substrate–metal distance, at the starting coordination complex is deleted.

All local minima (MINs), TSs, MSXs, and MECIs obtained after the above-mentioned two-step optimization procedure were re-optimized by CASPT2 with a larger aug-cc-pVDZ (AVDZ) basis set, where other parameters concerning the CASPT2 calculations are identical to those in the initial search. In MECI optimizations, the branching plane updating method was employed to avoid DCV calculations [32]. At all obtained stationary points, single point calculations at the CASPT2[14e, 13o] level with aug-cc-pVTZ (AVTZ) basis set were performed for better energetics, where singlet and triplet states were treated by MS- and SS-CASPT2, respectively, and the shift parameter 0.3 was applied. At MSX structures, spin–orbit coupling values were computed by the MRCISD[6e, 5o]/AVDZ method.

In initial AFIR search, optimization and reoptimization, all geometrical displacements were treated by a developmental version of the GRRM program [59]. Energy values and analytical gradient vectors were obtained by the Molpro2010 program [60, 61]. Spin–orbit coupling calculations were also performed by the Molpro2010 program. Single point energy calculations with the larger active space and basis set were performed by the Molcas7.4 program [62].

3. Results

Figure 1 lists all obtained structures at the CASPT2/AVDZ level. Energy values relative to the ground state reactants are shown below each structure, where CASPT2/AVTZ energy values are shown in parentheses. Although CASPT2/AVDZ with the small [6e, 5o] active space commonly underestimated relative energies by 10–30 kJ/mol for biradical species compared to those by CASPT2/AVTZ with the large [14e, 13o] active

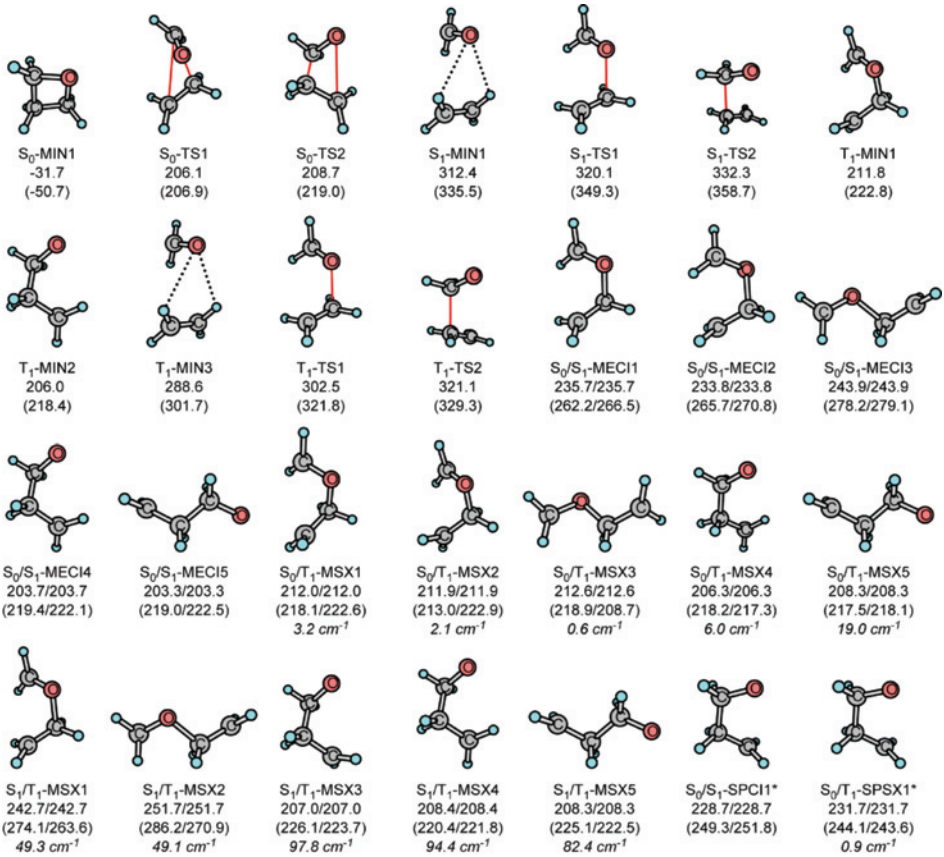

Fig. 1. Structures of all obtained MINs, TSs, MSXs, and MECIs in the automated AFIR search with the model collision energy $\gamma = 100$ kJ/mol, where S_0/S_1-SPCI1 and S_0/T_1-SPSX1 indicated by * were obtained separately for discussions (see text). Structures are optimized at the CASPT2[6e, 5o]/AVDZ level. Relative energy values to the ground state reactants pair are shown below each structure in kJ/mol, where CASPT2[14e, 13o]/AVTZ (single point) energies are shown in parentheses. In labels for MSX and MECI structures, energy values for both of two related states are shown. Spin–orbit coupling values in cm^{-1} by the MRCI[6e, 5o]/AVDZ calculations at MSX structures are given in italic. Cartesian coordinates for all these structures are available in Supporting Information.

space, qualitative discussions below based on the energetics by CASPT2/AVDZ are supported also by the CASPT2/AVTZ results. We note two saddles within SX and CI (S_0/T_1-SPSX1 and S_0/S_1-SPCI1) were obtained afterward to supplement discussions.

One recognizes on Fig. 1 that there are two types of biradical intermediates and crossings on T_1 and S_1: C–O–C–C type (T_1-MIN1, S_0/S_1-MECI1 to 3, S_0/T_1-MSX1 to 3, S_1/T_1-MSX1 and 2) and O–C–C–C type (T_1-MIN2, S_0/S_1-MECI4 and 5, S_0/T_1-MSX4 and 5, S_1/T_1-MSX3 to 5). For these two types, potential energy profiles are depicted on Fig. 2. When H_2CO is excited to the n-π^* S_1 state, it may either stay on S_1, undergoes internal conversion (IC) to S_0 or intersystem crossing (ISC) to T_1. Once decayed to S_0, the reaction of H_2CO with C_2H_4 has a very high barrier at S_0-TS1 or S_0-TS2

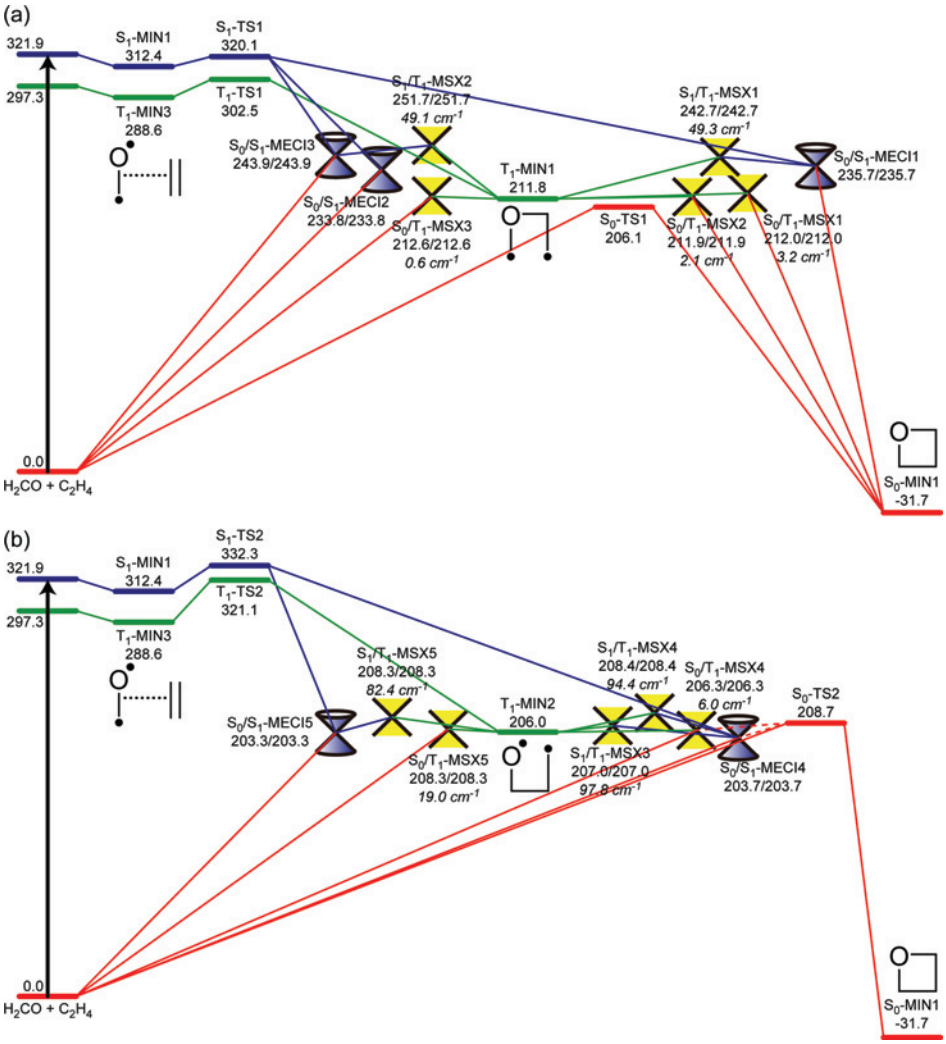

Fig. 2. Potential profiles for (a) the C–O–C–C biradical path and (b) the O–C–C–C biradical path, based on the energetics of CASPT2[6e, 5o]/AVDZ (in kJ/mol) in Fig. 1. At MSX structures, spin–orbit coupling values are shown in italic in cm^{-1}.

and will be very slow. On the other hand, when H_2CO stayed on S_1 or T_1 PES, there are two competing pathways leading either to the C–O–C–C or O–C–C–C biradical intermediate with formation of new O–C or C–C bond, respectively.

Figure 2a illustrates pathways *via* the C–O–C–C species. On S_1, there is no local minimum for biradical species, and the lowest energy point is located within the S_0/S_1-CI. The IRC from S_1-TS1 leads to near S_0/S_1-MECI1, and geometry optimization on S_0 starting from S_0/S_1-MECI1 converged to S_0-MIN1. This path represents one channel to the product S_0-MIN1. There are three MECIs of the C–O–C–C type (S_0/S_1-MECI1

to 3); the energy of S_1-TS1 is large enough to access all these MECIs. Although they may interconvert to each other easily, in this paper we did not study conformational rearrangement pathways. Both S_0/S_1-MECI2 and 3 dissociated to $H_2CO + C_2H_4$ during geometry optimizations on S_0; nonadiabatic transitions around these S_0/S_1-MECI2 and 3 let the system go back to the reactant pair, $H_2CO + C_2H_4$. On T_1, the IRC from T_1-TS1 reached T_1-MIN1. Around T_1-MIN1, there are five MSXs, S_0/T_1-MSX1 to 3 and S_1/T_1-MSX1 and 2, and all these can be accessed from T_1-TS1. When an ISC to S_0 occurs through S_0/T_1-MSX1 or 2, the product S_0-MIN1 is generated as confirmed by geometry optimizations on S_0 starting from them. S_0-MIN1 can also be reached from T_1-MIN1 after an ISC to S_1 through S_1/T_1-MSX1 and subsequent IC through S_0/S_1-MSX1. These give alternative pathways to the product. Other MSXs lead to regeneration of the reactant pair.

Figure 2b illustrates pathways *via* the O–C–C–C biradical. On S_1, the IRC from S_1-TS2 is connected to a region near S_0/S_1-MECI4. Similarly to the C–O–C–C species, the energy of S_1-TS2 is large enough to reach both S_0/S_1-MECI4 and 5. However, geometry optimization on S_0 starting from both S_0/S_1-MECI4 and 5 gave the reactants pair. Likewise, on T_1 both S_0/T_1-MSX4 and 5 were found to be connected to the reactants pair on S_0. These suggest that reproduction of the reactants pair is the more likely event after the C–C bond formation on both S_1 and T_1. This does not mean that the O–C–C–C species always go back to the reactants pair, because nonadiabatic transitions can take place high energy regions of SX/CI. Actually, both S_0/T_1-SX and S_0/S_1-CI can be extended to the region within the funnel of S_0-MIN, and representative points, S_0/S_1-SPCI1 and S_0/T_1-SPSX1, in the funnel are shown in Fig. 1. These are first-order saddle points within the S_0/S_1-CI and the S_0/T_1-SX hypersurfaces, respectively, and geometry optimizations on S_0 starting from them converged to S_0-MIN1. Hence, on Fig. 2 S_0/S_1-MECI4 and S_0/T_1-MSX4 are connected with S_0-TS2 by dashed lines. On the other hand, S_1-TS2 and T_1-TS2 are both higher in energy than their counterparts in Fig. 2a. This also suggests that contribution of the O–C–C–C biradical species is relatively minor in the present system.

4. Discussions

The important reaction pathways found in the present automatic reaction path search are summarized on Fig. 3. The same reaction system, $H_2CO + C_2H_4$, has been studied thoroughly in previous studies [49,50], and the present results are mostly consistent with these. Here, we point out a few differences between the present and the previous results. At first, in the previous study, there are very shallow local minima on S_0 for the C–O–C–C and O–C–C–C biradical species at the CASSCF[6e, 5o] level. These disappeared by inclusion of the dynamical electron correlation by the CASPT2[6e, 5o] method, although this change is trivial since TSs for dissociations of these biradicals are lower than those for generation of the product even at the CASSCF level. The other difference is that we found low-barrier TSs for generation of the biradical species on the excited states (*i.e.*, T_1-TS1, T_1-TS2, S_1-TS1, and S_1-TS2). These also show that O–C bond formation is more favorable than the C–C bond formation at the initial reaction step on the excited states. This is consistent with experimental observations for larger

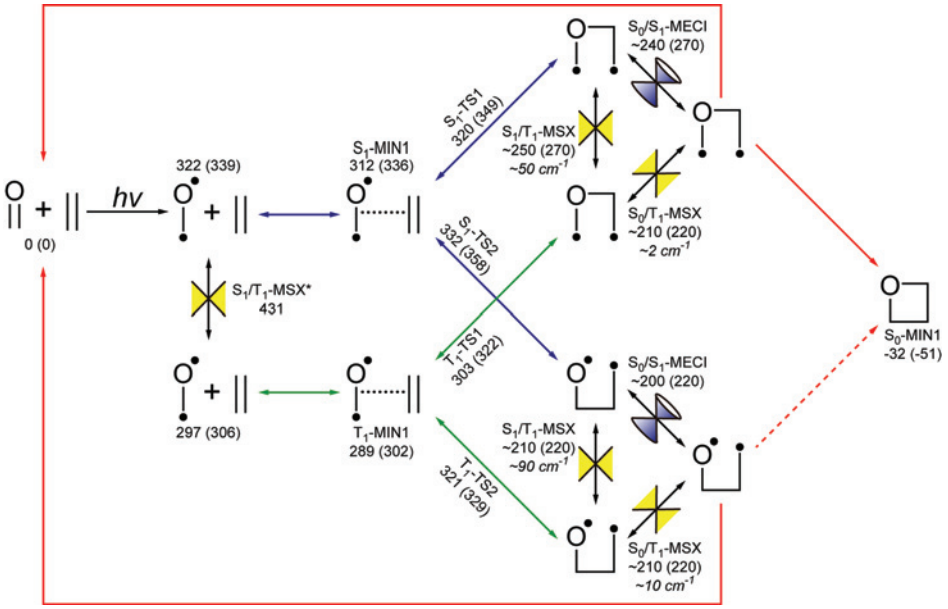

Fig. 3. An overview of reaction pathways for the Paternò–Büchi reaction obtained by the present automated reaction path search. Energy values (in kJ/mol) by CASPT2[6e, 5o]/AVDZ and CASPT2[14e, 13o]/AVTZ in parentheses are shown in each structure label. Spin–orbit coupling values are also presented for MSX structures. For simplicity, energies and spin–orbit couplings are averaged over similar MSX and MECI structures. S_1/T_1-MSX* is the lowest MSX between S_1 and T_1 PESs for isolated H_2CO taken from [56].

systems that O in aldehyde (or ketone) preferentially attaches to the less bulky site of alkene molecules. This selectivity would be conserved even in the minor O–C–C–C biradical routes. Since both S_0/S_1-MECI4 and S_0/T_1-MSX4 are located outside the funnel of S_0-MIN1, the final fate of the O–C–C–C biradical on S_0 should be controlled by the stability of S_0-TS2 for the final ring closure with the O–C bond formation.

As has been shown in the previous study on the C–O–C–C species on T_1 [50], spin–orbit coupling values between S_0 and T_1 on S_0/T_1-MSXs are very small. This is because S_0 and T_1 both have similar biradical electronic configurations. It follows that the lifetime of the C–O–C–C biradical on T_1 is long. This is consistent with experimental observations of the C–O–C–C intermediate [47] and that stereochemistry in alkene is lost by internal rotations of the long-lived C–O–C–C species on T_1. We suggest alternative escaping pathways from there through S_1/T_1-MSXs. As shown in Fig. 3, spin–orbit interactions with T_1 are much stronger for S_1 than for S_0. On S_1 the lobe for an unpaired electron at the terminal C or O atom in COCC or OCCC biradical, respectively, points a different direction compared to that for S_0 and T_1 [49], and this allows S_1 to have a large spin–orbit coupling with T_1. Thus, the ISC *via* high-lying S_1/T_1-MSXs with large spin–orbit couplings may compete with the ISC through low-lying S_0/T_1-MSXs with negligible spin–orbit couplings. Once moved to S_1 through S_1/T_1-MSXs, ultrafast IC to S_0 takes place through S_0/S_1-MECIs. On the other hand, the O–C–C–C biradical on T_1 can almost exclusively go through S_1/T_1-MSXs as these have high spin–

orbit couplings and are located only slightly above S_0/T_1-MSXs. The existence of the relatively fast ISC path through low-lying S_1/T_1-MSXs with high spin–orbit couplings suggests that the O–C–C–C biradical is a short lived intermediate compared to the C–O–C–C counterpart. It follows that stereochemistry in alkene might be maintained if a reaction which exclusively undergoes the O–C–C–C biradical path on T_1 is designed.

In contrast to the ISC, IC occurs much more quickly once a CI region is reached. Hence, in the singlet routes, stereochemistry in alkene is expected to be kept if further decay to T_1 does not take place. Indeed, the stereocheimistry has been found to be maintained when concentration of alkene is very high [44], and this has been attributed to the ultrafast IC at biradical states in the singlet routes. Whether singlet route or triplet route actually occurs is determined by the lifetime of S_1 of aldehyde (ketone) and collision frequency between the reactants. However, simulations of these are outside the scope of this study. In intramolecular PB reactions without the diffusion process of the reactants, contributions of the singlet routes would be high as the collision frequency between fragments should be higher than that for intermolecular reactions. When the reactants attached to each other on the S_1 PES, S_1/T_1-MSXs may again play a key role, since spin–orbital coupling values at these S_1/T_1-MSXs ($\sim 50\,cm^{-1}$) are large enough to cause a ultrafast ISC, according to a recent surface hopping simulation study [63]. Recent combined spectroscopic and *ab initio* studies did observed a ultrafast S_1 to T_1 ISC for some intramlecular PB reactions [54]. This ISC was explained by a crossing point between S_1 and a high-lying (repulsive) T_3 state outside the potential well of biradical intermediate found along a linear interpolation path between a S_0/S_1-CI and the Franck–Condon point, although no crossing with T_1 was further studied [54]. We suggest alternately that S_1/T_1-MSXs similar to those obtained in this study would have a significant role also in the ultrafast ISC observed for these intramlecular PB reactions. In intermolecular reactions, the stereochemistry of alkenes can be lost once moved to the long-lived T_1. Thus, in cases without randomization of the stereochemistry, the S_1/T_1 ISC would be very slow due to high energy S_1/T_1-MSXs and/or small S_1/T_1 spin–orbit couplings.

Finally, the present AFIR search was able to predict the PB reaction without using any estimate about its mechanism. Even the product was not assumed. Such a systematic search not only reproduced the previous results but also provided new insights into the present reaction. Of course, there still are limitations. First, choices of computation level, basis set, active space, *etc.* are crucial for obtaining reliable results, and it is still difficult to automate these choices especially in photoreactions involving electronic excited states. Second, the present method explores reaction pathways for a given system; in this study it was assumed that one H_2CO reacts with one C_2H_4. In reality, other reactant molecules as well as solvent molecules may assist reactions as intrinsic catalysts, and many combinations need to be considered in complex reactions. Third, dynamical effects associated with the nuclear kinetic energy are missing. The AFIR search gives a map of the minimum energy path connecting the critical points, MINs, TSs, MSXs, and MECIs. Although dynamical effects can be estimated and discussed by carefully looking at the map with a few additional calculations as has been done in this paper (see discussions on the saddle points within intersection seams SPCI and SPSX), for quantitative discussions dynamical simulations will be required. Nevertheless, the present approach would be very useful in future theoretical studies and predictions of the mech-

anism of photoaddition reactions. Another perspective is its application to prediction of the selectivity. For this purpose, use of the cheaper quantum chemical methods such as spin-flip-TD-DFT [64,65] is required in order to treat bulky substitution groups without simplification using less bulky groups. This is being tested for the PB reaction, and the results will be published elsewhere.

5. Conclusion

In this study, the PB photoaddition pathways for the simplest reactants $H_2CO + C_2H_4$ were explored systematically by the AFIR method. The AFIR search predicted all previously suggested pathways automatically. Although these pathways have been located in different studies and discussed separately, the present extensive set of reaction pathways gave a comprehensive view as illustrated in Fig. 3 and discussed in the last section. Especially, the ISC pathways between the triplet and singlet excited biradical species were found to play crucial roles in conventional triplet and singlet routes. It should be emphasized that in the present search we did not assume even the product of this reaction. Thus, the present approach would be promising for systematic study and *a priori* prediction of the mechanism of complex photoaddition reactions in future.

Acknowledgement

The authors thank to Dr. Yu Harabuchi and Mr. Ryohei Uematsu of Hokkaido University for helpful discussions. This work is partly supported by grants from Japan Society for the Promotion of Science (Grants-in-Aid for Scientific Research ⟨KAKENHI⟩ No. 23685004 at Hokkaido University and No. 24245005 at Kyoto University), as well as a grant from US AFOSR (Grant No. FA9550-10-1-0304) at Emory University. A part of calculations was performed using the computational resources in Institute for Molecular Science, Okazaki, Japan.

References

1. H. Eyring and M. Polanyi, Z. Phys. Chem. **12** (1931) 279.
2. H. B. Schlegel, J. Comput. Chem. **24** (2003) 1514.
3. F. Jensen, *Introduction to Computational Chemistry*, 2nd edn., Wiley, Chichester (2007).
4. H. B. Schlegel, WIREs Comput. Mol. Sci. **1** (2011) 790.
5. K. Fukui, J. Phys. Chem. **74** (1970) 4161.
6. K. Ishida, K. Morokuma, and A. Komornicki, J. Chem. Phys. **66** (1977) 2153.
7. K. Müller and L. D. Brown, Theor. Chim. Acta **53** (1979) 75.
8. M. Page and J. W. McIver Jr., J. Chem. Phys. **88** (1988) 922.
9. C. Gonzalez and H. B. Schlegel, J. Chem. Phys. **90** (1989) 2154.
10. H. P. Hratchian and H. B. Schlegel, J. Chem. Theory Comput. **1** (2005) 61.
11. N. Koga and K. Morokuma, Chem. Rev. **91** (1991) 823.
12. S. Niu and M. B. Hall, Chem. Rev. **100** (2000) 353.
13. M. Torrent, M. Solà, and G. Frenking, Chem. Rev. **100** (2000) 439.
14. T. Ziegler and J. Autschbach, Chem. Rev. **105** (2005) 2695.
15. K. N. Houk and P. H.-Y. Cheong, Nature **455** (2008) 309.
16. S. Kato, R. L. Jaffe, A. Komornicki, and K. Morokuma, J. Chem. Phys. **78** (1983) 4567.

17. N. Koga and K. Morokuma, Chem. Phys. Lett. **119** (1985) 371.
18. D. Schröder, S. Shaik, and H. Schwarz, Acc. Chem. Res. **33** (2000) 139.
19. R. Poli and J. N. Harvey, Chem. Soc. Rev. **32** (2003) 1.
20. F. Bernardi, M. Olivucci, and M. A. Robb, Chem. Soc. Rev. **25** (1996) 321.
21. D. R. Yarkony, Acc. Chem. Res. **31** (1998) 511.
22. L. Sobolewski, W. Domcke, C. Dedonder-Lardeux, and C. Jouvet, Phys. Chem. Chem. Phys. **4** (2002) 1093.
23. B. G. Levine and T. J. Martínez, Annu. Rev. Phys. Chem. **58** (2007) 613.
24. S. Nanbu, T. Ishida, and H. Nakamura, Chem. Sci. **1** (2010) 663.
25. M. R. Manaa and D. R. Yarkony, J. Chem. Phys. **99** (1993) 5251.
26. M. J. Bearpark, M. A. Robb, and H. Bernhard Schlegel, Chem. Phys. Lett. **223** (1994) 269.
27. J. M. Anglada and J. M. Bofill, J. Comput. Chem. **18** (1997) 992.
28. C. Ciminelli, G. Granucci, and M. Persico, Chem. Eur. J. **10** (2004) 2327.
29. T. W. Keal, A. Koslowski, and W. Thiel, Theor. Chem. Acc. **118** (2007) 837.
30. F. Sicilia, L. Blancafort, M. J. Bearpark, and M. A. Robb, J. Chem. Theory Comput. **4** (2008) 257.
31. B. G. Levine, J. D. Coe, and T. J. Martínez, J. Phys. Chem. B **112** (2008) 405.
32. S. Maeda, K. Ohno, and K. Morokuma, J. Chem. Theory Comput. **6** (2010) 1538.
33. A. Migani, A. Sinicropi, N. Ferré, A. Cembran, M. Garavelli, and M. Olivucci, Faraday Discuss. **127** (2004) 179.
34. O. Weingart, A. Migani, M. Olivucci, M. A. Robb, V. Buss, and P. Hunt, J. Phys. Chem. A **108** (2004) 4685.
35. T. Mori and T. J. Martínez, J. Chem. Theory Comput. **9** (2013) 1155.
36. S. Maeda, K. Ohno, and K. Morokuma, Phys. Chem. Chem. Phys. **15** (2013) 3683.
37. S. Maeda and K. Morokuma, J. Chem. Phys. **132** (2010) 241102.
38. S. Maeda and K. Morokuma, J. Chem. Theory Comput. **7** (2011) 2335.
39. S. Maeda, S. Komagawa, M. Uchiyama, and K. Morokuma, Angew. Chem. Int. Ed. **50** (2011) 644.
40. S. Maeda and K. Morokuma, J. Chem. Theory Comput. **8** (2012) 380.
41. S. Maeda, E. Abe, M. Hatanaka, T. Taketsugu, and K. Morokuma, J. Chem. Theory Comput. **8** (2012) 5058.
42. E. Paterno and G. Chiefi, Gazz. Chim. Ital. **39** (1909) 341.
43. G. Büchi, C. G. Inman, and E. S. Lipinsky, J. Am. Chem. Soc. **76** (1954) 4327.
44. L. Kürti and B. Czakó, *Strategic Applications of Named Reactions in Organic Synthesis*, Elsevier B.V., Amsterdam (2005).
45. N. Hoffmann, Chem. Rev. **108** (2008) 1052.
46. H. Zimmerman, Science **153** (1966) 837.
47. S. C. Freilich and K. S. Peters, J. Am. Chem. Soc. **103** (1981) 6255.
48. A. G. Griesbeck, H. Mauder, and S. Stadtmueller, Acc. Chem. Res. **27** (1994) 70.
49. I. J. Palmer, I. N. Ragazos, F. Bernardi, M. Olivucci, and M. A. Robb, J. Am. Chem. Soc. **116** (1994) 2121.
50. A. G. Kutateladze, J. Am. Chem. Soc. **123** (2001) 9279.
51. A. G. Griesbeck, M. Abe, and S. Bondock, Acc. Chem. Res. **37** (2004) 919.
52. Y. Yabuno, Y. Hiraga, R. Takagi, and M. Abe, J. Am. Chem. Soc. **133** (2011) 2592.
53. M. D'Auria, Tetrahedron **68** (2012) 8699.
54. R. Y. Brogaard, O. Schalk, A. E. Boguslavskiy, G. D. Enright, H. Hopf, V. Raev, E. Tarcoveanu, T. I. Sølling, and A. Stolow, Phys. Chem. Chem. Phys. **14** (2012) 8572.
55. M. A. Collins, Theor. Chem. Acc. **108** (2002) 313.
56. S. Maeda, K. Ohno, and K. Morokuma, J. Phys. Chem. A **113** (2009) 1704.
57. S. Maeda, R. Saito, and K. Morokuma, J. Phys. Chem. Lett. **2** (2011) 852.
58. S. Maeda, K. Ohno, and K. Morokuma, Adv. Phys. Chem. **2012** (2012) 268124.
59. S. Maeda, Y. Osada, K. Morokuma, and K. Ohno, *GRRM, a Developmental Version* (AFIR is not available currently in the distribution version GRRM11), Hokkaido University (2013).
60. H.-J. Werner, P. J. Knowles, G. Knizia, F. R. Manby, and M. Schütz, WIREs Comput. Mol. Sci. **2** (2012) 242.,

61. MOLPRO, Version 2010.1, a Package of ab initio Programs, H.-J. Werner, P. J. Knowles, G. Knizia, F. R. Manby, M. Schütz, P. Celani, T. Korona, R. Lindh, A. Mitrushenkov, G. Rauhut, K. R. Shamasundar, T. B. Adler, R. D. Amos, A. Bernhardsson, A. Berning, D. L. Cooper, M. J. O. Deegan, A. J. Dobbyn, F. Eckert, E. Goll, C. Hampel, A. Hesselmann, G. Hetzer, T. Hrenar, G. Jansen, C. Köppl, Y. Liu, A. W. Lloyd, R. A. Mata, A. J. May, S. J. McNicholas, W. Meyer, M. E. Mura, A. Nicklass, D. P. O'Neill, P. Palmieri, D. Peng, K. Pflüger, R. Pitzer, M. Reiher, T. Shiozaki, H. Stoll, A. J. Stone, R. Tarroni, T. Thorsteinsson, and M. Wang, see http://www.molpro.net.
62. F. Aquilante, L. De Vico, N. Ferré, G. Ghigo, P.-Å. Malmqvist, P. Neogrády, T. B. Pedersen, M. Pitonak, M. Reiher, B. O. Roos, L. Serrano-Andrés, M. Urban, V. Veryazov, and R. Lindh, J. Comput. Chem. **31** (2010) 224.
63. M. Richter, P. Marquetand, J. González-Vázquez, I. Sola, and L. González, J. Phys. Chem. Lett. **3** (2012) 3090.
64. Y. Shao, M. Head-Gordon, and A. I. Krylov, J. Chem. Phys. **118** (2003) 4807.
65. N. Minezawa and M. S. Gordon, J. Phys. Chem. A **113** (2009) 12749.